PROTON STRUCTURE FUNCTIONS AND THE GLUON DISTRIBUTION

R. LAHMANN
DESY-H1
Notkestr. 85
22607 Hamburg, Germany
E-mail: lahmann@mail.desy.de

Recent experimental results from H1 and ZEUS are presented with respect to their contribution to the understanding of the inner structure of the proton. With the large 1997 statistics, the proton structure function F_2 has been measured with remarkable precision over a wide kinematic range. At high values of Q^2, effects due to the Z^0 and $W^\pm$ bosons have been observed. Furthermore, new results of the longitudinal proton structure function F_L and the charm contribution $F_2^{c\bar{c}}$ to F_2 are discussed. Finally, measurements of the gluon distribution from F_2 scaling violations, charm production and dijet events are presented and compared. All results are well described within the framework of QCD.

1 Introduction

The measurement of the inclusive neutral current deep inelastic scattering (DIS) cross section $\sigma(ep \to eX)$ has been one of the prime tasks of the H1 and ZEUS detectors at HERA. Its precise determination is essential for an investigation of the proton structure and for precision tests of QCD. The double differential DIS cross section is parameterized by the generalized structure functions F_i according to

$$\frac{d^2\sigma^{e^\pm p}}{dxdQ^2} = \frac{2\pi\alpha^2}{Q^4 x}[Y_+ F_2(x,Q^2) - y^2 F_L(x,Q^2) \mp Y_- xF_3(x,Q^2)], \qquad (1)$$

where $Y_\pm = 1 \pm (1-y)^2$. Q^2 is the squared four-momentum transfer between the lepton and the proton and x is the Bjorken variable. The inelasticity is defined as $y = Q^2/(xs)$, where the squared center-of-mass energy $s = 4E_eE_p$ is derived from the electron[a] and proton beam energies E_e and E_p. In 1997, with beam energies of $E_e = 27.5$ GeV and $E_p = 820$ GeV, the resulting $\sqrt{s} \approx 300$ GeV allowed double differential measurements up to $Q^2 \lesssim 20\,000$ GeV^2.

The generalized structure functions F_2 and F_L contain contributions from both virtual photon and Z^0 exchange. For $Q^2 \ll M_Z^2$, where M_Z is the mass of the Z^0 boson, only the virtual photon contribution is relevant. In this case,

[a]HERA operated with positrons between 1994 and 1997. The expression 'electron' will be used throughout this paper to refer to both electrons and positrons.

F_2 and F_L can be approximated by their electromagnetic components F_2^{em} and F_L^{em}, respectively, while the parity violating contribution xF_3 becomes negligible. In the quark parton model (QPM), these structure functions are then given by $F_2^{em}(x) = x\sum_{i=1}^{n_f} e_i^2[q_i(x) + \overline{q}_i(x)]$ and $F_L^{em} = 0$ for spin $\frac{1}{2}$ partons. In perturbative QCD, gluon distributions are taken into account and F_2^{em} is calculated from a convolution of the parton distributions and a set of corresponding coefficient functions.

2 Measurement of F_2

The kinematic variables y (or x) and Q^2 can be determined from the electron, the hadronic final state, or from a combination of both. The ZEUS collaboration uses the double angle method [1], in which the polar angle of the hadronic jet and of the electron are combined to reconstruct the event kinematics. The H1 collaboration employs the electron method, where

$$Q_e^2 = 4E_eE_e{}'\cos^2\frac{\theta_e}{2} \quad \text{and} \quad y_e = 1 - \frac{E_e{}'}{E_e}\sin^2\frac{\theta_e}{2}\ . \tag{2}$$

Here $E_e{}'$ and θ_e are the energy and polar angle of the scattered electron, respectively. For both the H1 and the ZEUS detector reference frames are used where the electron beam has a polar angle of $\theta = 180°$. The region near the beam pipe in electron direction is termed the "backward region".

A convenient quantity is the reduced cross section σ_r, defined as

$$\sigma_r \equiv \frac{d^2\sigma^{e^\pm p}}{dQ^2dx}\cdot\frac{Q^4x}{2\pi\alpha^2Y_+} = F_2 - \frac{y^2}{Y_+}F_L \mp \frac{Y_-}{Y_+}xF_3\ . \tag{3}$$

which at low values of y and Q^2 approaches the proton structure function F_2.

New preliminary measurements of F_2 from H1 and ZEUS have been presented recently [2,3,4,5]. The key components of the ZEUS detector for the analysis are the uranium scintillator calorimeter (UCAL) and the central tracking detector (CTD). The data used for the 1996-1997 F_2 analysis correspond to an integrated luminosity of 6.8 pb^{-1} (mostly taken during 1996) in the low Q^2 region and 27.4 pb^{-1} (mostly taken during 1997) in the high Q^2 region. ZEUS defines the region $Q^2 \leq 22$ GeV^2 as the low and $Q^2 \geq 27$ GeV^2 as the high Q^2 region.

For the H1 detector, the separation of the high and low Q^2 region is given by the detector instrumentation. Depending on whether the electron is scattered into the central region, which is instrumented with a Liquid Argon Calorimeter (LAr) or into the backward region equipped with a lead-fiber

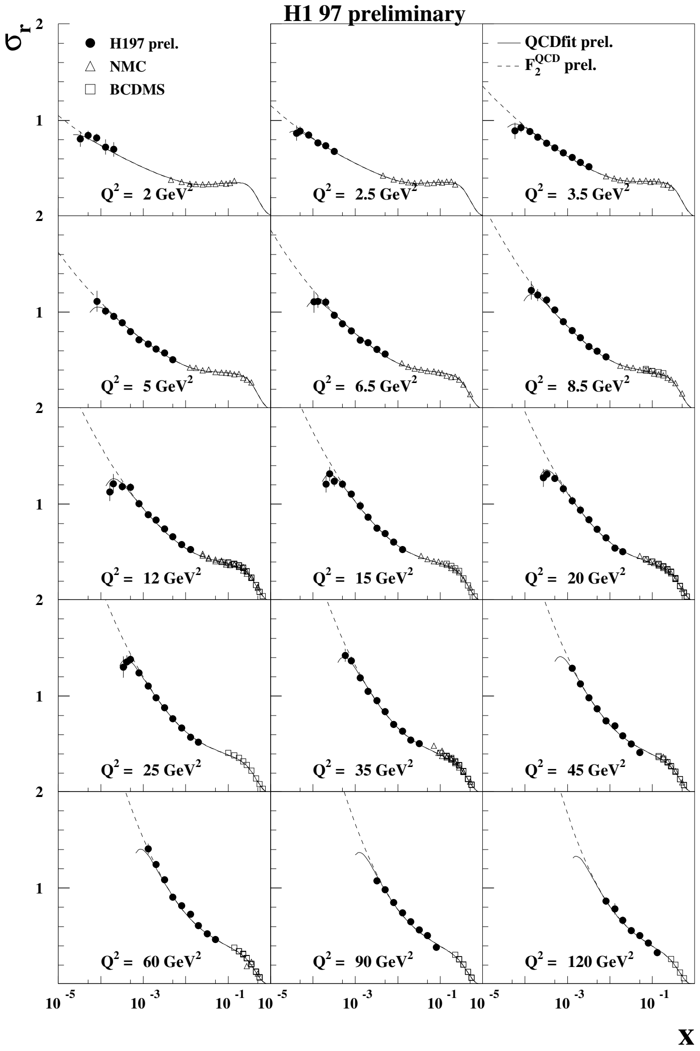

Figure 1: H1 measurement of the reduced DIS cross section (full circles) as a function of x for fixed Q^2, compared to a NLO QCD fit to the H1, NMC, and BCDMS data (solid line). The dashed curve is the F_2 structure function determined with this fit.

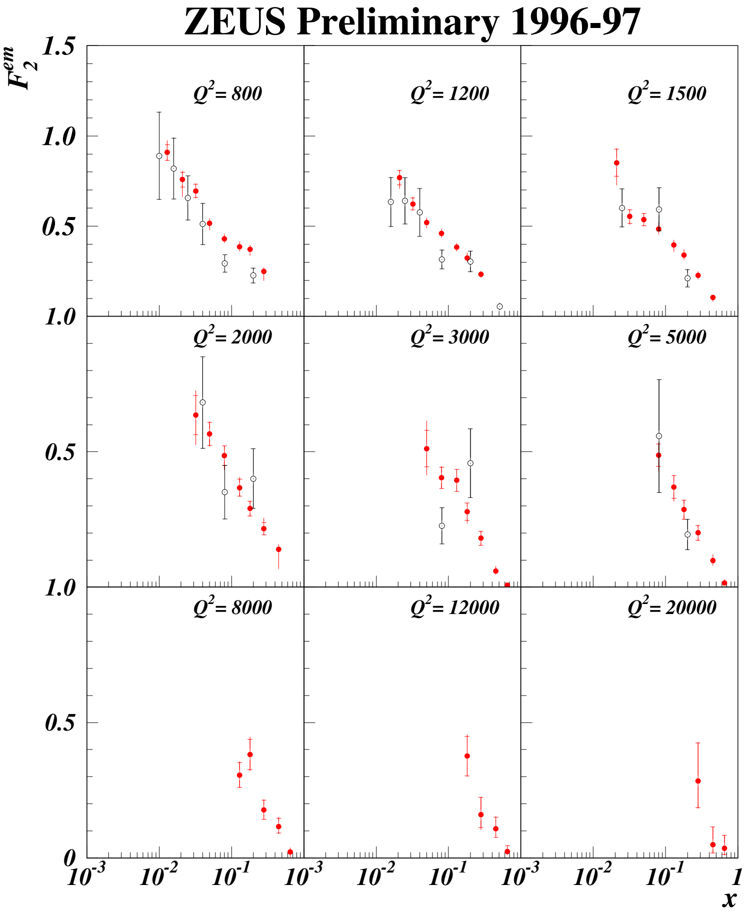

Figure 2: ZEUS measurement of F_2^{em} as a function of x for fixed Q^2 (in GeV^2). The full circles and dashed bars correspond to the measurement described in the text, the open circles and solid bars show the 1994 ZEUS results. The inner error bars show the statistical errors, the outer error bars the quadratic sum of statistical and systematic errors.

calorimeter (SPACAL), the events are said to have high or low Q^2, respectively. Tracking is done with the central tracker and with a planar Backward Drift Chamber (BDC) in the respective regions. For $Q^2 < 20$ GeV^2 the newly installed Backward Silicon Tracker (BST) has been used for tracking and background rejection.

In 1997, H1 recorded an integrated luminosity of 15 pb^{-1} in the range 10 GeV$^2 < Q^2 \leq 120$ GeV^2, and of 2 pb^{-1} in the range 2 GeV$^2 \leq Q^2 < 10$ GeV^2 in a dedicated run with specific trigger settings. In the high Q^2 region with $Q^2 \geq 200$ GeV^2, the H1 analysis uses an integrated luminosity of 37.0 pb^{-1} collected from 1994 to 1997.

The cross section is determined by converting the number of events counted in bins of x and Q^2 , after background subtraction, into a bin averaged cross section using Monte Carlo acceptance calculations. In the low Q^2 region, main contributions to the systematic error of the cross section measurement result from the energy calibration (systematic studies require large statistics, e.g. cell-by-cell calibration and local effects) and photoproduction background. The 1997 luminosity more than doubles the previously existing luminosity and allowed measurements of F_2 with systematic errors of 3–5% and statistical errors of 1–2%. for the measurement of F_2 at low Q^2.

In figure 1, the preliminary measurement of the reduced cross section with 1997 data from H1 is shown. One can observe a smooth transition to the fixed target data at large x and a steep rise of F_2 towards low x. Both H1 and ZEUS have performed NLO QCD fits to their F_2 data, using the DGLAP [6] evolution equations for three light flavors and adding the charm contribution determined in the NLO calculation of the boson gluon fusion process [7]. The agreement between the data and a NLO QCD fit to the H1, NMC [8], and BCDMS [9] experimental data performed by H1 can be seen to be very good. The departure of the reduced cross section from the behavior of F_2 for high y is attributable to the contribution of F_L.

Since the electromagnetic part of the double differential DIS cross section is proportional to $1/Q^4$, the statistics decreases rapidly with increasing Q^2. For the H1 measurements with the 1997 data in the high Q^2 region typical systematic errors are about 8%. For $Q^2 \gtrsim 1000$ GeV^2, the precision is still limited by the statistical error. One finds a good agreement between the data and a NLO QCD fit.

The electromagnetic part F_2^{em} of the structure function F_2 as measured by ZEUS is shown in figure 2. One can observe the improvement in precision resulting from the increased statistics of the 1997 HERA operation. At the high Q^2 values shown in this figure, contributions of the Z^0 boson to F_2 are

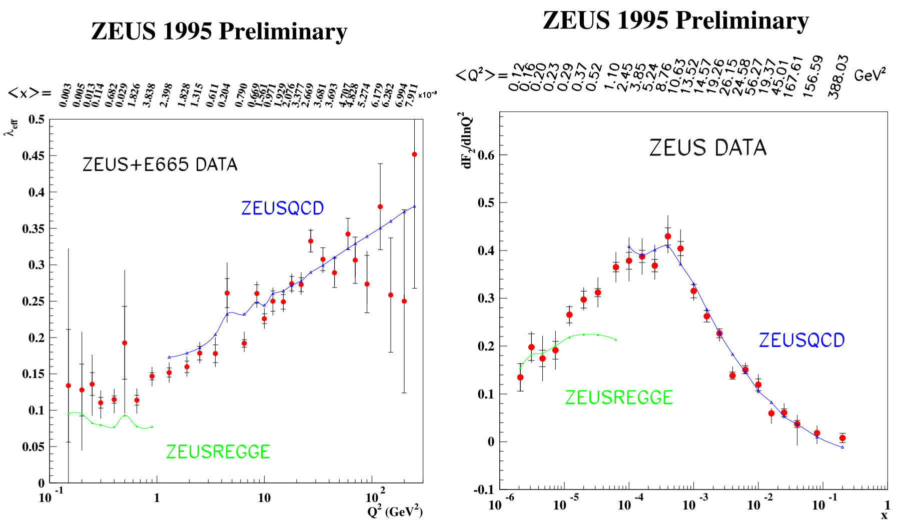

Figure 3: Measurement by the ZEUS collaboration of the parameter λ described in the text (left) and of the slope $F_2 = a + b \ln Q^2$ (right). Left plot: In a Q^2 bin, $\langle x \rangle$ is calculated from the weighted means of $\ln(1/x)$ ($\langle x \rangle$ ranging from 0.003 to 7.911 $\times 10^{-3}$). Right plot: In a x bin, $\langle Q^2 \rangle$ is calculated from the weighted means of $\ln Q^2$ ($\langle Q^2 \rangle$ ranging from 0.12 to 388.03 GeV^2). The inner error bars represent the statistical errors, the outer bars the quadratic sum of all contributions to the error. Also shown are fits to the data based on different models as described in the text.

not negligible and the xF_3 term[b] of the double differential cross section has to be taken into account. Above $Q^2 = 800$ GeV^2, the statistical errors grow typically to 5–15% and dominate the total error.

2.1 F_2 Slopes: $d \ln F_2 / d \ln(1/x)$ and $d \ln F_2 / d \ln Q^2$

For fixed values of Q^2, the low x behavior of F_2 can be characterized by $F_2 \propto \lambda^{-x}$, where the value of λ assumes quite different values in the Regge [10] and BFKL [11] approaches. The effective value of λ for $x < 0.01$, calculated from the weighted mean value of $\ln(1/x)$ in a given Q^2 bin, has been measured by H1 and ZEUS. In order to reach the low x values needed to test the Regge theory, the ZEUS collaboration has included E665 data[12]. Results from ZEUS are shown in figure 3. The fact that λ is greater than zero means that F_2 is rising with decreasing x, even at lowest Q^2. For $Q^2 \gtrsim 1$ GeV^2, F_2 rises

[b]Note that for e^+p scattering, the minus sign of the xF_3 term in equation 1 applies.

stronger for higher values of Q^2. For $Q^2 \lesssim 1$ GeV^2, the rise flattens out and approaches the Regge expectation of $\lambda \approx 0.1$.

Also shown in figure 3 is a fit $F_2 = a + b \ln Q^2$ in bins of fixed x from the ZEUS collaboration, allowing a quantitative investigation of the scaling violations. ZEUS has performed a DL [10] style Regge fit for very low x and Q^2 values and a QCD fit for $Q^2 > 1$ GeV^2. The latter describes the turnover of the data at $x \approx 3 \times 10^{-4}$ quite well. This turnover can be understood in terms of the different behavior of the gluon and $q\bar{q}$ sea distributions at $Q^2 \approx 1$ GeV^2 [4].

2.2 Measurements at Very Low Q^2

The interest in the transition between the region of perturbative QCD (DIS) and photoproduction described by Regge phenomenology has lead both H1 and ZEUS to extend the measurement of the proton structure to the lowest possible Q^2 regions.

In order to reach values as low as $Q^2 = 0.35$ GeV^2, HERA was operating with the interaction point shifted by 70 cm into the forward direction during a part of 1995. Furthermore, the HERA experiments have instrumented the region very close to the beam pipe in the backward direction. ZEUS has installed the Backward Proportional Chamber (BPC) in 1995, which has delivered results ranging down to $Q^2 \approx 0.1$ GeV^2. H1 is currently in the process of starting up its Very Low Q^2 (VLQ) detector.

H1 has used radiative events to investigate the kinematic region down to $Q^2 \approx 0.2$ GeV^2 [13]. With this method, the cross section of highly radiative events $\sigma(ep \to e\gamma X)$ is measured, where the photon is detected by a tagger in the HERA tunnel, about 100 m upstream from the H1 detector in electron direction. Since the energy of the interacting electron is reduced by the energy of the photon, Q^2 is reduced proportionally to the reduction of the electron energy (compare equation 2). With this method, roughly 8000 events (corresponding to an integrated luminosity of 3 pb^{-1}) from the 1996 data set have been analyzed. Using a newly available Monte Carlo program including complete $\mathcal{O}(\alpha^4)$ calculations for one tagged photon [14], the systematic errors of the measurement are about 20%.

In figure 4, the F_2 measurements at very low Q^2 are compared for the various methods used by the H1 and ZEUS collaborations. The agreement between the different measurements is very good. Shown in the figure are also two different fits to the data. A Regge based DL fit describes the data only in the lowest Q^2 bin with an acceptable precision and shows an increasing disagreement with the data for increasing values of Q^2. The NLO QCD fit shows very good agreement in its range of application.

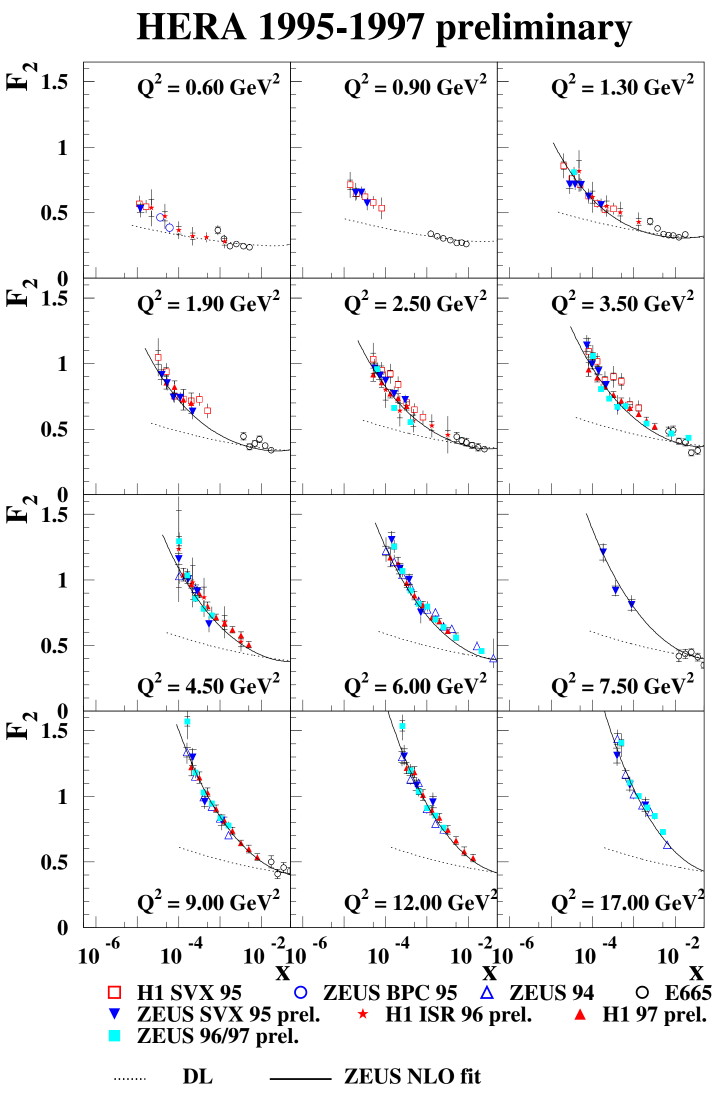

Figure 4: The structure function F_2 in the very low Q^2 region as measured by H1 and ZEUS using the different methods described in the text. Also shown are fits to the data using a Regge based DL model (dotted line) and a NLO QCD fit (solid line).

2.3 Effects of the Z^0 and $W^\pm$ Bosons at High Q^2

The sensitivity of the neutral current differential cross section $d\sigma/dx$ to the γZ^0 interference becomes significant for $Q^2 \gtrsim 10\,000$ GeV^2 [5, 15]. While still limited in statistics, both H1 and ZEUS data shows good agreement with the electroweak standard model and disfavor a purely electromagnetic neutral current.

Charged current events in e^+p scattering are characterized by a large imbalance of the total measured transverse momentum due to the presence of the anti-neutrino. Single and double differential cross sections have been measured in the kinematic region $Q^2 \gtrsim 400$ GeV^2 [5, 16]. The number of events which pass the selection cuts for the charged current analysis from 1994 to 1997 are 933 for ZEUS and about 700 for H1.

Differential cross sections $d\sigma/dx$ for bins ranging from $Q^2 = 400$ GeV^2 to $Q^2 = 16\,000$ GeV^2 for H1 and $Q^2 = 530$ GeV^2 to $Q^2 = 17\,000$ GeV^2 for ZEUS have been parameterized by the underlying valence and sea quark distributions. The data show good agreement with the Standard Model and a sensitivity to the dominance of the valence quark (sea quark) contribution at high (low) values of x.

3 Determination of F_L

The determination of F_L is possible only at high values of y where the term involving F_L in equation 3 becomes sizeable with respect to F_2. The effect of F_L on the reduced cross section could be observed in figure 1. In order to determine F_L under the current HERA conditions of fixed beam energies, the H1 group has employed two methods [2, 17]. First, the conventional "subtraction" method, where the value of F_2 extrapolated with a DGLAP evolution equation is subtracted from the measured reduced cross section to obtain $F_L = Y_+/y^2(F_2 - \sigma_r)$. Second the new "derivative" method: Defining the derivative $\partial\sigma_r/\partial\log y$ as

$$\left.\frac{\partial\sigma_r}{\partial\log y}\right|_{Q^2} = -\frac{\partial F_2}{\partial\log x} - F_L \cdot 2y^2 \cdot \frac{2-y}{Y_+^2} + \frac{\partial F_L}{\partial\log x} \cdot \frac{y^2}{Y_+} \tag{4}$$

one can determine F_L in a new way with increased sensitivity to F_L with respect to the F_2 part. The new method is demonstrated and results from both methods are shown in figure 5. Both methods show consistent results and are consistent with F_L as calculated using a NLO QCD fit to F_2. With the derivative method, lower values of Q^2 can be reached since the assumption on F_2 is not based on QCD.

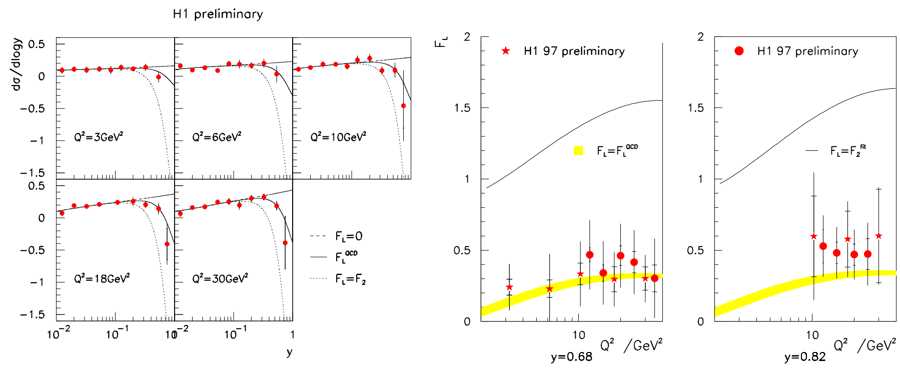

Figure 5: Left hand side: Measurement of the derivative $\partial\sigma_r/\partial\log y$. The curves represent the QCD cross section fit result (solid curve), and the fit result with the replacements $F_L = 0$ (dashed curve, basically a straight line) and $F_L = F_2$ (dotted curve). Right hand side: Determination of F_L using the subtraction method (full circles) and the derivative method (stars) for two different values of y. The narrow band represents the uncertainty range of F_L when calculated using the gluon and quark distributions determined with the NLO QCD fit to the H1, NMC and BCDMS data. The solid line represents the QCD cross section fit result with the replacement $F_L = F_2$. In all plots, the inner error bars represent the statistical errors and the total error bars represent the quadratic sum of statistical and systematic errors.

4 The Charm Contribution $F_2^{c\bar{c}}$ to F_2

The dominant process of $c\bar{c}$ production in DIS is boson gluon fusion in which a photon coupling to the incoming electron interacts with a gluon in the proton to form a $c\bar{c}$ pair. The relation between the cross section of charm production in DIS ($\sigma^{c\bar{c}}$) and $F_2^{c\bar{c}}$ is given by substituting σ and F_2 in equation 1 by the corresponding expressions. The contribution of the $F_L^{c\bar{c}}$ term is expected to be on the order of $1 \sim 2$ % in the kinematic region explored by the analyzes described in the following and therefore has been neglected.

Conventionally, $\sigma^{c\bar{c}}$ has been measured by both H1 and ZEUS through the decay $c \to D^{*\pm} \to (K^{\mp}\pi^{\pm})\pi^{\pm}$ [18, 19]. Here the $D^{*\pm}$ is tagged using the tight kinematic constraints of the decay chain. The $D^{*\pm}$ cross section is deduced from the number of events observed in bins of Q^2 and x or y after background and efficiency corrections from Monte Carlo calculations. The charm cross section is then obtained by correcting the $D^{*\pm}$ cross section by the hadronization fraction of charm to $D^{*\pm}$ and by the branching ratio for the decay $D^{*\pm} \to (K^{\mp}\pi^{\pm})\pi^{\pm}$.

Recently, ZEUS has presented a measurement of $F_2^{c\bar{c}}$ using semileptonic

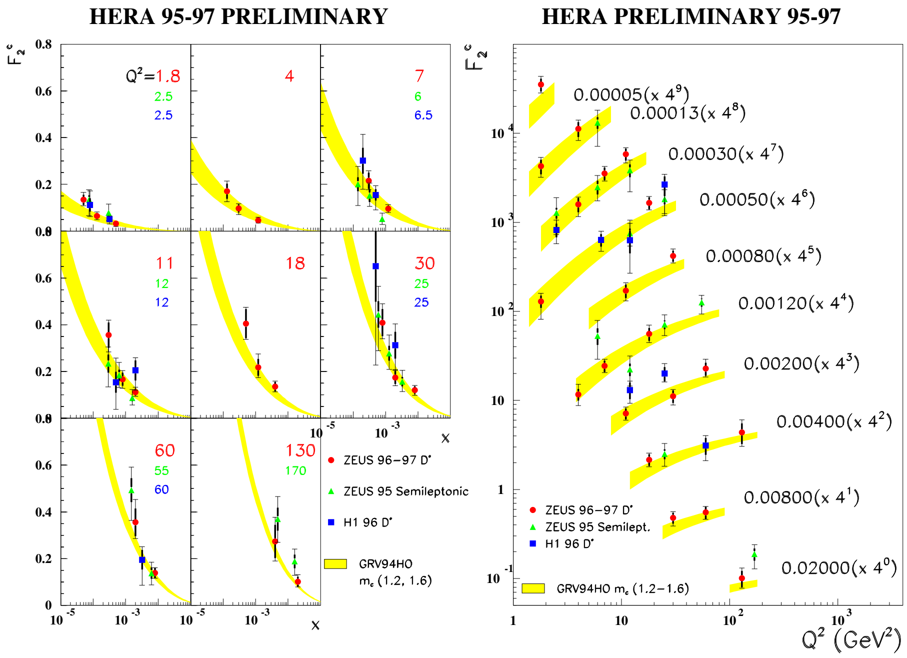

Figure 6: Measurement of $F_2^{c\bar{c}}$ from H1 and ZEUS and comparison to a NLO QCD calculations with the GRV94 HO [21] parton distribution functions as input (shaded band). The inner error bars show the statistical error and the outer ones the quadratic sum of the statistical and experimental error. Left hand side: $F_2^{c\bar{c}}$ as a function of x for fixed values of Q^2. Right hand side: $F_2^{c\bar{c}}$ as a function of Q^2 for fixed values of x.

charm decays in DIS [20]. In this analysis, the inclusive e^- signal[c] is identified, after suitable background subtraction, as originating from the semileptonic decays of hadrons containing a charm quark. The extraction of $F_2^{c\bar{c}}$ in bins of Q^2 and x then follows along the lines described above for the $D^{*\pm}$ analysis.

In the left part of figure 6 the results for $F_2^{c\bar{c}}$ from H1 and ZEUS are compared as a function of x for fixed values of Q^2. One observes a good agreement for the different methods and for the two experiments. If one expresses $F_2^{c\bar{c}}$ as a fraction of F_2 one obtains a sizeable contribution of $F_2^{c\bar{c}}$ to the proton structure function of the order $0.1 \lesssim F_2^{c\bar{c}}/F_2 \lesssim 0.3$ in the kinematic range of figure 6.

In the right part of figure 6, $F_2^{c\bar{c}}$ is shown as a function of Q^2 for constant

[c] e^+ signals are excluded since this sample is contaminated with scattered beam positrons.

x. Again, one observes good agreement between the measurements of the two experiments. Qualitatively, the same scaling violating behavior as for F_2 can be observed.

5 The Gluon

5.1 The Gluon Density from Scaling Violations

The most precise way to determine the gluon density $x \cdot g(x)$ is from the scaling violations of F_2 which are due to gluon *bremsstrahlung* from quarks and quark pair production from gluons. The parameterization of the gluon distribution is contained in the NLO QCD fits to F_2 described in section 2. H1 and ZEUS use slightly different parameterizations of the parton densities and starting points for the evolution; details can be found elsewhere [2, 4].

The results from H1 and ZEUS are shown in figure 7, together with the results from NMC and some global distributions. One can observe a steep rise of $x \cdot g(x)$ for decreasing x and a good agreement between H1 and ZEUS.

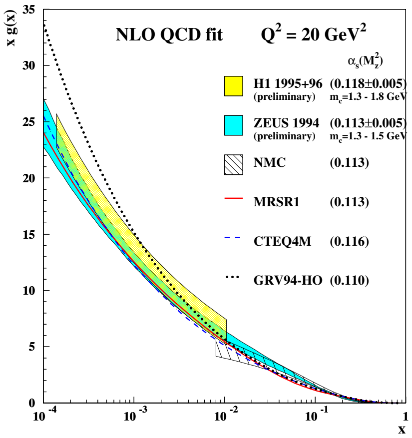

Figure 7: Gluon distributions from the HERA NLO QCD fits to the structure function data. ZEUS has recently presented new gluon distributions [4] which are not yet included in the plot. The error bands include the statistical and systematic errors. The NMC fit is also shown at higher x. The MRSR1 [22], CTEQ4M [23], and GRV94 HO [21] parameterizations are shown for comparison.

5.2 The Gluon Density from Charm Production

H1 has determined the gluon density from charm production in DIS and photoproduction [24] within the framework of the NLO QCD programs HVQDIS [25] and FMNR [26], respectively. In leading order of the process $\gamma g \to c\bar{c}$, the momentum fraction in the infinite momentum frame is given by $x_g = (M^2 + Q^2)/ys$, where M is the invariant mass of the $c\bar{c}$ system. The *observed* gluon density x_g^{OBS} is different from x_g due to the presence of gluon radiation and the experimental conditions, under which not charm quarks but D^* mesons are measured.

The measurement of the gluon density proceeds in two main steps: First, the visible D^* cross section is measured as a function of x_g^{OBS}. Second, the gluon density at the "true" x_g is extracted from the observed cross section and the observed gluon density by means of an unfolding integral after subtraction of the quark-induced contribution to the visible cross section.

The resulting gluon densities at an average scale $\mu^2 = 25\ \mathrm{GeV}^2$ are shown in figure 8. One can observe a good agreement between the gluon densities extracted from the photoproduction and DIS D^* analysis. The agreement with the gluon density obtained from the F_2 scaling violations is also good.

5.3 The Gluon Density from Dijet Cross Sections

Dijet production is sensitive to the gluon density through the formation of quark–antiquark pairs by the process of boson gluon fusion described above. In a recent analysis [27] the gluon density was derived from a NLO QCD fit to the DIS dijet cross sections, using a value of $\alpha_s(M_Z^2) = 0.119 \pm 0.005$, and performing a simultaneous fit to the inclusive neutral current DIS ep-cross sections (compare section 2) to constrain the quark density in the proton. Jets were formed with the "longitudinally boost invariant $k_\perp$ algorithm" [28, 29] in the range $10\ \mathrm{GeV}^2 < Q^2 < 5000\ \mathrm{GeV}^2$. In the leading order picture, the gluon density is probed at the fractional proton momentum ξ which is equivalent to the variable x_g from the previous subsection with M replaced by the invariant mass of the dijet system. The analysis was performed at a factorization scale $\mu_f^2 = 200\ \mathrm{GeV}^2$ in the range $0.01 < \xi < 0.1$; The preliminary result of the analysis is shown in figure 9.

The kinematic range extends to higher values of x compared to the gluon density derived from the F_2 scaling violations. One finds good agreement in the region of overlap.

6 Summary

H1 and ZEUS have presented new structure function data with improved precision. For $Q^2 \lesssim 100\ \mathrm{GeV}^2$, F_2 has been measured with a systematics dominated error of $\lesssim 5\%$. The F_2 data is well described by NLO QCD fits up to the largest accessible values of $Q^2 \approx 20\,000\ \mathrm{GeV}^2$. At high values of y, effects on the reduced cross section due to F_L become visible. The deviation of the reduced cross section from the expected value of F_2 has been used to determine F_L. The results show good agreement with calculations of F_L using a NLO QCD fit to F_2. At high Q^2 values, effects due to the Z^0 and $W^\pm$ bosons have

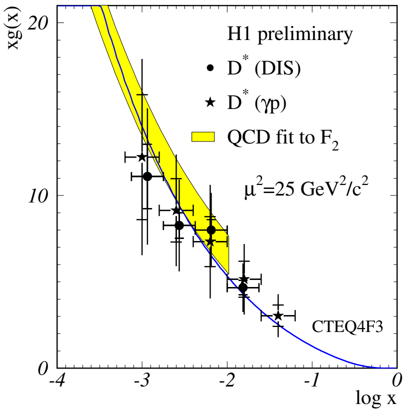

Figure 8: Comparison of the gluon densities obtained from the D^* analysis with the H1 results from scaling violations and the CTEQ4F3 parameterization. The systematic error is the quadratic sum of all contributions, dominated by the uncertainties of the charm quark mass and the fragmentation parameter. The inner error bar is the statistical error.

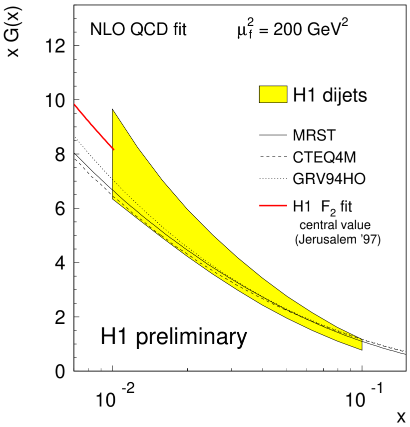

Figure 9: The gluon density in the proton from a NLO QCD fit to dijet cross sections. The error band is compared to the gluon densities obtained in different global analyzes and to the central value of the H1 gluon density from scaling violations.

been observed by the HERA experiments which show good agreement with the Standard Model. For the charm contribution $F_2^{c\bar{c}}$ to F_2, new results are available which are in good agreement with NLO QCD.

The gluon density in the proton has been measured using different independent methods. The most precise measurements are from the F_2 scaling violations. Here the results from H1 and ZEUS show good agreement and show a steep rise of the gluon density for decreasing values of x. Measurements of the gluon density have also been obtained from the analysis of charm and dijet events. These measurements extend the kinematic range of the measurement to lower values of x and show good agreement with the results from the scaling violations in the region of overlap.

Acknowledgments

I would like to thank the spokespersons of H1 and ZEUS for allowing me to participate in RADCOR98. Many thanks also to my colleagues from H1 and ZEUS who provided the material needed for my presentation. Special thanks to M. Klein for his help with my presentation and this paper.

References

1. S.Bentvelsen, J.Engelen, P. Kooijman in: Physics at HERA, vol.1, 23 (1991); K.C. Hoeger, in: Physics at HERA, vol.1, 43 (1991).
2. H1 Collab., paper 534 contributed to the ICHEP 98 conference.
3. ZEUS Collab., paper 769 contributed to the ICHEP 98 conference.
4. ZEUS Collab., paper 770 contributed to the ICHEP 98 conference.
5. H1 Collab., paper 533 contributed to the ICHEP 98 conference.
6. Yu.L. Dokshitzer, *Sov. Phys. JETP* **46**, 641 (1977);
   V.N. Gribov and L.N. Lipatov, *Sov. J. Nucl. Phys.* **15**, 438 and 675 (1972); G. Altarelli and G. Parisi, *Nucl. Phys.* B **126**, 298 (1977).
7. E. Laenen *et al.*, *Nucl. Phys.* B **392**, 162 (1993);
   S. Riemersma *et al.*, *Phys. Lett.* B **347**, 143 (1995).
8. NMC Collab., M.Arneodo *et al.*, *Nucl. Phys.* B **483**, 3 (1997).
9. BCDMS Collab., A.C. Benvenuti *et al.*, *Phys. Lett.* B **223**, 485 (1989).
10. A.Donnachie and P.V. Landshoff, *Z. Phys.* C **61**, 139 (1994).
11. Y. Balitzki and L. Lipatov *Sov. J. Nucl. Phys.* **28**, 822 (1978);
    E. Kuraev, L. Lipatov and V. Fadin *Sov. Phys. JETP* **45**, 199 (1977).
12. E665 Collab., M.R. Adams *et al.*, *Phys. Rev.* D **54**, 3006 (1996).
13. H1 Collab., paper 535 contributed to the ICHEP 98 conference.
14. H. Anlauf *et al.*, hep-ph/9805384.
15. ZEUS Collab., paper 752 contributed to the ICHEP 98 conference.
16. ZEUS Collab., paper 751 contributed to the ICHEP 98 conference.
17. H1 Collab., S.Aid *et al.*, *Phys. Lett.* B **393**, 452 (1997).
18. H1 Collab., paper 540 contributed to the ICHEP 98 conference.
19. ZEUS Collab., paper 768 contributed to the ICHEP 98 conference.
20. ZEUS Collab., paper 772 contributed to the ICHEP 98 conference.
21. M. Glück, E.Reya and A. Vogt, *Z. Phys.* C **67**, 433 (1995).
22. A. Martin, R. Roberts and W. Stirling, DTP/96/44, RAL-TR-96-037.
23. H.L. Lai *et al.*, *Phys. Rev.* D **55**, 1280 (1997).
24. H1 Collab., paper 538 contributed to the ICHEP 98 conference.
25. B.W. Harris and J. Smith, preprint DESY 97-111, FSU-HEP-970527, May 1997.
26. S. Frixione *et al.*, *Phys. Lett.* B **348**, 633 (1995); *Nucl. Phys.* B **454**, 3 (1995).
27. H1 Collab., paper 520 contributed to the ICHEP conference.
28. S.D. Ellis and D.E. Soper, *Phys. Rev.* D **48**, 3160 (1993).
29. S. Catani, Yu.L. Dokshitzer, M.H. Seymour and B.R. Webber, *Nucl. Phys.* B **406**, 187 (1993).